Computers in Biology and Medicine 126 (2020) 104012

Contents lists available at ScienceDirect

Computers in Biology and Medicine

journal homepage: http://www.elsevier.com/locate/compbiomed

Computational frame of ligament *in situ* strain in a full knee model

Malek Adouni [a,b,*], Tanvir R. Faisal [f], Yasin Y. Dhaher [a,c,d,e]

[a] Northwestern University, Physical Medicine and Rehabilitation Department, 345 East Superior Street, Chicago, IL, 60611, United States
[b] Australian College of Kuwait, Mechanical Engineering Department, East Meshrif, P.O. Box 1411, Kuwait
[c] Department of Physical Medicine and Rehabilitation, University of Texas Southwest, Dallas, TX, United States
[d] Department of Orthopedic Surgery, University of Texas Southwest, Dallas, TX, United States
[e] Bioengineering, University of Texas Southwest, Dallas, TX, United States
[f] Department of Mechanical Engineering, University of Louisiana at Lafayette, LA, 70508, USA

ARTICLE INFO

Keywords:
In situ strain
Ligaments
Knee
Finite element
Optimization

ABSTRACT

The biomechanical function of connective tissues in a knee joint is to stabilize the kinematics-kinetics of the joint by augmenting its stiffness and limiting excessive coupled motion. The connective tissues are characterized by an *in vivo* reference configuration (*in situ* strain) that would significantly contribute to the mechanical response of the knee joint. In this work, a novel iterative method for computing the *in situ* strain at reference configuration was presented. The framework used an *in situ* strain gradient approach (deformed reference configuration) and a detailed finite element (FE) model of the knee joint. The effect of the predicted initial configuration on the mechanical response of the joint was then investigated under joint axial compression, passive flexion, and coupled rotations (adduction and internal), and during the stance phase of gait. The inclusion of the reference configuration has a minimal effect on the knee joint mechanics under axial compression, passive flexion, and at two instances (0% and 50%) of the stance phase of gait. However, the presence of the ligaments *in situ* strains significantly increased the joint stiffness under passive adduction and internal rotations, as well as during the other simulated instances (25%, 75% and 100%) of the stance phase of gait. Also, these parameters substantially altered the local loading state of the ligaments and resulted in better agreement with the literature during joint flexion. Therefore, the proposed computational framework of ligament *in situ* strain will help to overcome the challenges in considering this crucial biological aspect during knee joint modeling. Besides, the current construct is advantageous for a better understanding of the mechanical behavior of knee ligaments under physiological and pathological states and provide relevant information in the design of reconstructive treatments and artificial grafts.

1. Introduction

The mechanical functions of knee ligaments guide and restrict the joint movement. The functions of these tissues have been determined based on knee cadaveric studies using successive ligament eliminations to measure the overall load or local strain in the ligaments [1–7]. Additionally, these organs are characterized by *in vivo* reference configuration in the absence of any external loading, and they respond accordingly when subjected to a specific well-distributed internal strain (*in situ* strain). This inner property of the soft tissues has been classified into two categories: pre-strain (initial strain) and stress-free (residual strain) configurations. Experimental observations have shown that the pre-strain in the ligaments and its associated stress are relieved when the ligament is removed from the joint; thus, they yield a relatively stress-free configuration that can provide insight into the residual strains [8]. The *in situ* strains (pre-strain and stress-free) of the knee ligaments have been observed in the range of 1–10% [3,9,10] and are considered to be essential parameters affecting the joint's stability [11,12]. These parameters lead to a null reaction around the boundaries of the structure to balance the complete absence of external loading. Consequently, the *in situ* strains must be non-uniformly distributed and should be elaborated through a theoretical frame depending on the geometry [3].

Generally, two frames accommodating the *in situ* strain in the soft tissues are considered during the computational investigations. One structure is based on the deformation of the stress-free configuration to determine the stress in a reference case [8]. In this frame, the stress map

* Corresponding author. Physical Medicine and Rehabilitation Department, 355 East Superior Street Chicago, IL 60611.
E-mail addresses: malek.adouni@northwestern.edu, malek.adouni@polymtl.ca (M. Adouni).

https://doi.org/10.1016/j.compbiomed.2020.104012
Received 4 July 2020; Received in revised form 14 September 2020; Accepted 17 September 2020
Available online 7 October 2020

of the stress-free configuration, that is, the residual strain and initial geometry, is assumed to be known. This represents a massive limitation in the application of the previous frame. In practical situations, the determination of the residual strain can be challenging, and there is no guarantee that it exists within the ligament [13]. In the other frame, which is well-known as the deformed reference configuration, there is no requirement for the stress-free setup since this option is absorbed by the deformation gradient covering the reference case [8]. This deformation gradient can be obtained using an analytical solution [14], indirectly from experimental data [15] or by solving an inverse finite element (FE) problem [16]. Most published studies have supported the second frame more than the first frame, and this is due to the less observed numerical singularity and the promising predicted results with this scheme. However, one of the significant limitations facing the deformed reference configuration is that it does not provide evidence for the system's full equilibrium under the predicted *in situ* strain [17]. Integrating the process of calculating the gradient of soft tissue deformation at the reference configuration into the auto-balance process of the full joint may help in obtaining safe predictions. The objective of this study was to develop and implement a computational framework to estimate the *in situ* strain of ligaments in a full knee finite element model. The structure used a pre-strain gradient approach (deformed reference configuration) and a three-dimensional knee joint model. The "best" distributions of the initial ligament stretch (*in situ* stretch) leading to an optimal reference configuration under a minimal knee reaction load were calculated. Subsequently, the effect of this estimated initial configuration on the mechanical response of the joint was investigated.

2. Methods

2.1. Finite elements model

A finite element model of the entire knee joint, consists of all relevant soft tissues, was employed [15] (Supplementary Materials section: Fig. 1). The model includes three well-aligned bony structures (tibia, femur, and patella) simulated as a rigid body due to their much higher stiffness compared with associated articular cartilage layers and menisci [18]. Reduced integration hexahedral continuum-based representation was used to model the articular cartilage and menisci. The same representation was employed to simulate patellar tendon (PT), quadriceps tendon (QT) and the six principal ligaments, anterior/posterior cruciate ligaments (ACL/PCL), lateral/medial collateral ligaments (LCL/MCL) and lateral/medial patellofemoral ligaments (LPFL/MPFL). The existing meshes of tibial, femoral and patellar articular cartilages were further refined extensively for better accuracy. In addition, the element local coordinate system was created to incorporate the exact mapping of the collagen networks and the variation of the properties of the depth-dependent solid matrix. In the superficial zone of cartilage, the collagen fibrils are oriented horizontally, parallel to the medial and lateral directions. In the transitional zone of the cartilage, fibrils are randomly oriented (i.e., no dominant orientations) following a gradual curvature starting parallel from the superficial zone and turning perpendicular to the surface (along with the medial and lateral directions). In the deep zone, vertical fibrils are initially oriented perpendicular to the subchondral junction [19]. In menisci, element properties vary along the circumferential and radial directions based on the local coordinate system (Supplementary Materials section: Fig. 5). Ligament interaction and articulation at the cartilage/meniscus and cartilage/cartilage are simulated using a surface to surface frictionless contact algorithm (A detailed description of the FE model is demonstrated in the subsection "FE model description" of the Supplementary Materials section).

2.2. Material properties

The PT and QT were assumed to be neo-hookean with material coefficients (C_{10}) 55.9 MPa for the PT and 65.9 MPa for the QT [20]. A transversely isotropic, linearly elastic, homogeneous material [21] was considered for the menisci. The circumferential modulus was set at 120 MPa, and the axial and transverse moduli were assumed to be identical and were set at 20 MPa. The circumferential, radial and axial Poisson's ratios were set to 0.45, 0.3, and 0.3, respectively [22–25]. A value of 0.001 g/mm^3 was assigned for the density of all the soft tissues [26], whereas the bony structures were assigned with a density of 0.002 g/mm^3 [27].

Multiplicative decomposition of the deformation gradient into elastic and plastic parts is introduced here to create the fibrils reinforced composites model of cartilage (Supplementary Materials section: Fig. 4). Therefore, the proposed model is considered as hierarchical hyper-elasto-plastic composite material starting from the tropocollagen molecules level (300 nm) to continuum macro-level (+100 μm). Fundamentally, for soft tissues, the plastic flow is associated only with the uniaxial deformation of the collagen fibril [28,29]. Thereafter, the yield strength of the fibril is a function of crosslink density between tropocollagen molecules, defined herein as the density function g_0 (β) (Supplementary Materials section: eq. 7). Coarse-graining procedure is employed to link the nanoscale collagen features and the tissue level materials properties, using the crosslink density function as a building block. Generalized neo-hookean strain energy is used to model the micro-fibrils, fibrils and tissue behavior by considering the rule of mixtures (for more details on the formulation of the material see the Supplementary Material section (eqs. 5-14) and our prior works [30–32]). Cartilage collagen fibrils volume fractions of 15, 18 and 21% are considered in superficial, transitional and deep zones, respectively [33]. To reflect the incompressibility of the articular cartilage during the transient (short-term) biphasic response, an equivalent elastic response was sought by using equilibrium (drained) modulus of the tissue and Poisson's ratio of 0.5 [34]. The drained modulus was considered depth-dependent, varying from 0.3 to 1.2 MPa when descending from the surface to the lowermost layer at the subchondral bone, respectively [35].

For the ligaments (ACL, PCL, MCL, LCL, MPFL, LPFL), a transversely isotropic hyperelastic material model, assumed to be nearly incompressible [15], driven by an uncoupled representation of the strain energy function, defined by Limbert and Middleton [36], was employed (Supplementary Materials section: eqs. 1-4). In this framework, the fibers were anticipated to be extensible and uniformly distributed in the ground substance and perfectly bonded to the matrix, while the matrix was assumed to be isotropic and hyperelastic. With the proposed strain energy function, the typical nonlinear stiffening behavior of the collagen fibers under tension is provided by an exponential form and the collagen fibers are assumed not to support any compressive loads. The joint sensitivity response to this material formulation and its validation were previously investigated [15] and the best sets of material parameters were considered in the present investigation. The detailed description of the model was demonstrated in the supplementary material section and our prior works [15,37–39]. In the current study, the *in situ* strains are considered as the initial stretches along the local fibers-directions (λ_0). These components were included in the FE model of the ligaments by defining three different configurations using the theory of the deformed reference configuration scheme [40]: the stress-free state, the reference state, and the current state. Using the multiplicative decomposition, the total deformation gradient can be defined as $F_c = F_0\, F_r$, where F_0 is the deformation gradient from the stress-free state to the reference state (the initial stretch in the ligaments) and F_r is the deformation gradient from the reference state to the current state (see supplementary material Fig. 3). The initial stretch field is assumed to be an uni-axial stretch with$F_0 = diago[\lambda_0\ \sqrt[-1]{\lambda_0}\ \sqrt[-1]{\lambda_0}]$. The parameter λ_0 was determined through an optimization process described in the following section. It is noteworthy that during this investigation, the above mentioned transverse hyperelastic scheme was considered due to multiple factors. These

Table 1
Parameters considered in the GA optimization.

Description of function	Value
Population size	330
Creation function	Feasible population
Selection	Roulette
Elite count	33
Crossover fraction	0.88
Mutation	Adaptive feasible
Crossover	Intermediate
Hybrid function	fmincon
Generations	380
Function tolerance	1e-6

factors are the absence of the real geometry of the ligaments in case of free boundary conditions, lack of initial guess or any tested experimental data on the full auto-balance of the knee joint in the absence of external loading, the reported high distortion of the elements associated with other methods such as stress-free configuration, and finally the observed agreement on the accuracy of the scheme in predicting *in situ* strain especially for joint ligaments [8,41].

2.3. Ligaments In situ strain

2.3.1. Problem formulation

The essential elements for the optimization formulation are the set of design variables, the objective function, and the constraints. The design variables included all the *in situ* strains (initial stretches) of the ligaments and were represented by a vector X (eq. (1)) as follows.

$$X_{\{i=33\}} = \left[\lambda_{0_{ACL\ \{i=6\}}},\ \lambda_{0_{PCL\ \{i=2\}}},\ \lambda_{0_{MCL\ \{i=18\}}},\ \lambda_{0_{LCL\ \{i=3\}}},\ \lambda_{0_{LPFL\ \{i=2\}}},\ \lambda_{0_{MPFL\ \{i=2\}}}\right]. \quad (1)$$

The geometrical distribution i (ligament partitions) was designed based on the available data in the literature [3,4,7,8,42–50] and was adjusted (the ACL from 4 to 6 and the MCL from 15 to 18) to improve the convergence rate. Using binary alphabet structure, these design variables were encoded as strings to be considered as chromosomes of the adopted GA.

In our current knee joint model, we have two sub joints, the tibiofemoral joint connecting the femur to the tibia and the patellofemoral one connecting the femur to the patella. Each joint is characterized by six degrees of freedom (3 translations: anterior-posterior, medial-lateral and proximal-distal, and 3 rotations: flexion extension, adduction-abduction and internal-external (medial-lateral tilt for the patella)), which result in the 12° of freedom of the knee joint. Hence, the objective function (f) is built with regard to the 12° of freedom of the knee joint under a given excitation of the initial stretches X. This function was represented by the sum of the generated tibial and patellar reactions (eq. (2)).

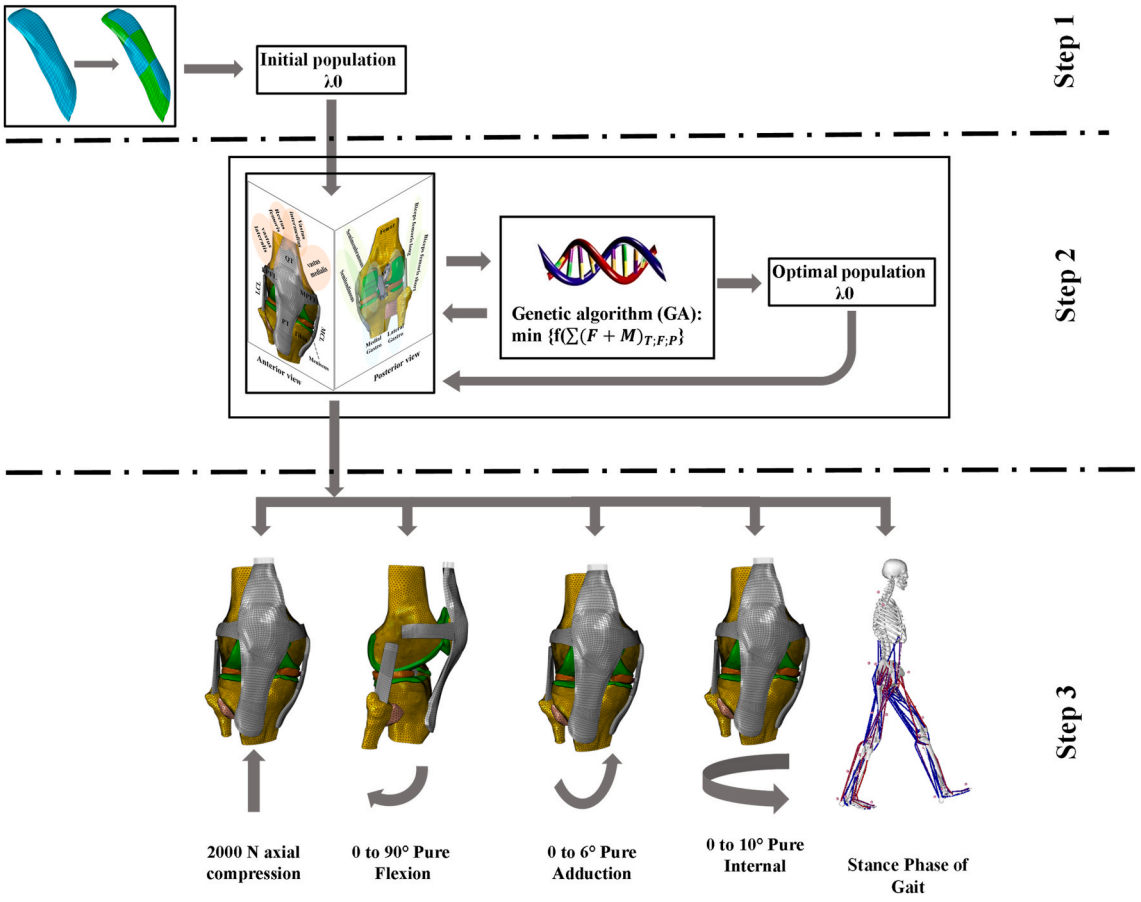

Fig. 1. A flow diagram explaining the optimization process associated with the knee FE model to figure out the optimal population of ligaments *in situ* strains and the different boundary conditions followed to investigate their effect on the joint biomechanics. Three steps have been followed during this process, step (1), ligaments partitions to define the geometrical distributions of the ligament *in situ* strains (33 areas), step (2), the call of the FE model (fitness function) iteratively from the GA algorithm to determine the optimal set of ligament *in situ* strains, step (3) investigate the effect of the optimal set of ligament *in situ* strains under isolated and daily activates. The 3D finite element model of the knee joint include all the soft tissues such as anterior cruciate ligaments (ACL), posterior cruciate ligaments (PCL), medial and lateral collateral ligament (MCL, LCL), lateral patellofemoral (LPFL), medial patellofemoral (MPFL), quadriceps tendon (QT) and patellar tendon (PT) cartilage layers, menisci and also including all the muscles surrounding the knee joint.

Table 2
Simulated loading cases.

Loading Case	Applied Boundary conditions to the tibial bone	
	Force/ Displacements	Constraints
Axial compression	2000 N	Only flexion/extension Fixed
Pure Adduction	6°	Flexion/extension and Internal/external Fixed
Pure internal	10°	Flexion/extension and Adduction/ Abduction Fixed
Pure flexion	90°	Tibial bone free, except the prescribed rotations (flexion)
Stance phase	OpenSim	Prescribed rotations of the instances [39]

$$\left\{ f(X) = \sum_{j=1,2,3} \left(F_{Tibia} + F_{patella}\right)_j + \sum_{j=1,2,3} \left(M_{Tibia} + M_{patella}\right)_j \right\}_{\text{estimated using FE model}} \quad (2)$$

Where F and M stand for the reaction forces and moments in the anatomical coordinate system ($j = 1$, anterior-posterior axis; $j = 2$. medial-lateral axis; and $j = 3$, proximal-distal axis), respectively. The value of the objective function was calculated for each iteration at full extension position corresponding to the minimum activation of muscle forces surrounding the knee joint.

The adopted constraints limit the values of the design variables (*Xi*). Several inequalities (k represent the number of ligaments) ensure a positive initial average stretch (for each ligament) and an upper limit that is not exceeding the reported maximum initial strains (10%) [8] (eq. (3)).

$$0.3\% \leq avreage\left\{\lambda_{0\{each\ ligament\}}\right\}_{k=6} \leq 10\% \quad (3)$$

2.3.2. Optimization process

A built-in genetic algorithm (GA) code from the MATLAB optimization toolbox was utilized in the present study and the associated steps were as follows: (1) A population with random gene values was created. (2) The algorithm was terminated when the best fitness in successive iterations no longer produced better results based on the FE model. (3) The roulette wheel principle was used to select the participants in crossover and mutation operations. (4) The offspring individuals were obtained from parent individuals using genetic procedures (crossover and mutation). (5) The entire population was evaluated (2) and based on the evaluation, a certain number of individuals are chosen to survive for the next iteration. (6) When the genetic algorithm was terminated to improve the value of the fitness function, "Fmincon" was used as a hybrid function. The parameters considered during the optimization process have been summarized in Table 1. These parameters have been determined after several iterations testing the fitness function by varying the parameters of the genetic algorithm, such as population size, initial range, elite account, crossover fraction, and generation. The individual or combined action of variation, as well as the range of variation of the algorithm parameters, have been fixed considering the provided guidance of the Matlab help center and global optimization toolbox. The same technique was also implemented in our prior works to ensure the global minima of the muscle forces optimization during the stance phase of gait [51,52] (Fig. 1).

2.4. Loading and boundary conditions

To explore the effect of the estimated *in situ* strain on the joint aggregate mechanics, the knee joint response was computed for five different loading conditions (Fig. 1); 2000 N axial compression at full knee extension, six degrees of passive adduction and ten degrees of passive internal rotation at full extension, tibial passive flexion starting from full extension until 90° flexion and the five instances (0%: initial contact, 25%: loading response, 50%: midstance, 75%: terminal stance

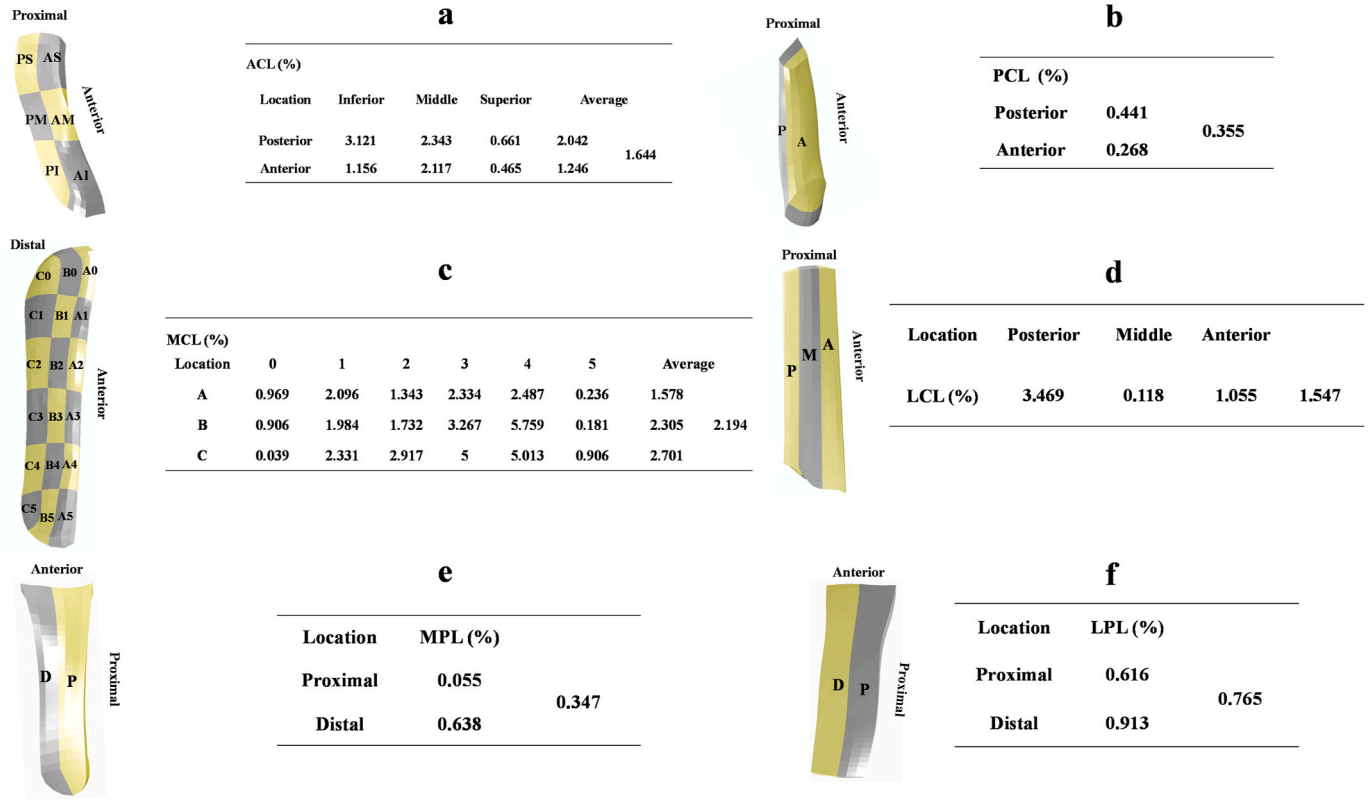

Fig. 2. The optimum sets of the ligaments *in situ* strains predicted by the optimization process; ACL (a), PCL (b), MCL (c), LCL (d), MPFL (e), LPFL (f).

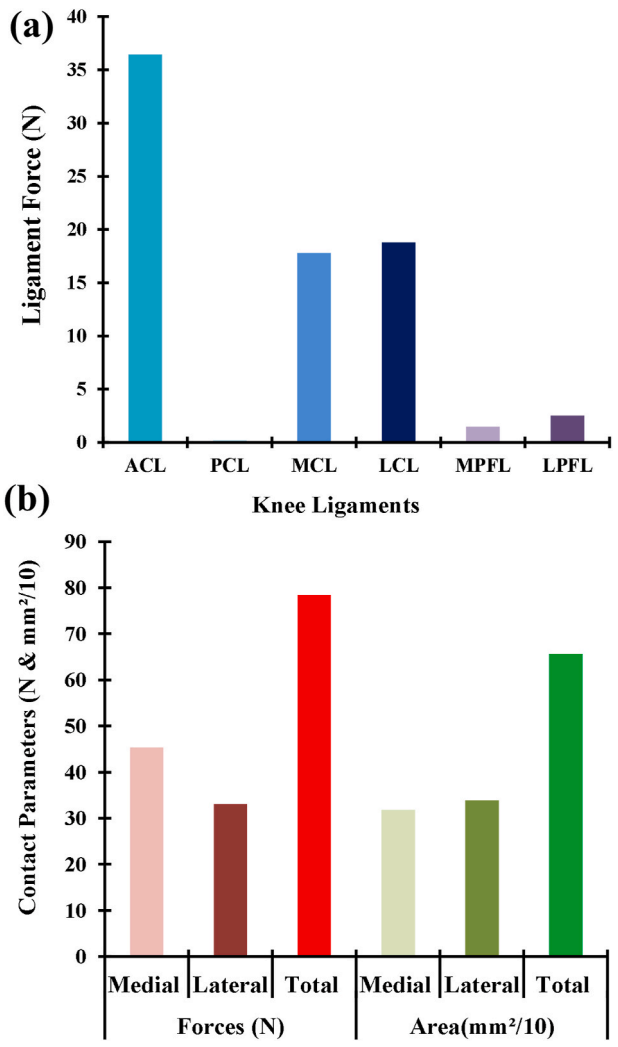

Fig. 3. The predicted (a) ligaments forces and (b) contact parameters at full extension when the joint under the reaction of the ligaments *in situ* strains without any external load.

and 100%: pre-swing) of the stance phase of the gait cycle (Table 2). The lower limb rotations, moments, knee muscle forces, and ground reaction forces at foot during the stance phase are based on our *in vivo* measurements for healthy subjects [39]. Knee muscle forces from the musculoskeletal modeling simulations (OpenSim) were prescribed as distributed surface traction loads along the line of actions across their insertion sites, except the gastrocnemius. Because the femur was fixed in space during the analysis, the forces from the muscles inserting on the femur were prescribed alternately. Through the use of experimentally measured joint angles, forces from the gastrocnemius were replaced by an equivalent force and moment system acting on the reference node of the TF joint center in the local TF coordinate system. The contributions of the ground reaction forces and moments to the knee joint were prescribed based on calculations of knee joint torques and forces using inverse dynamics in the local coordinate system.

Due to the absence of the deformable state of the knee passive tissues during the optimization of the muscle forces using the musculoskeletal model of OpenSim, additional higher moments were computed within the FE model. A corrective measure has been followed [51,52] to determine the updated response of the muscle forces surrounding the knee joint. This correction was done iteratively by counterbalancing the updated moments in deformed configurations. For each iteration, the knee reaction moments were computed based on the optimized muscle forces (applied as external loads), and the procedure was iterated 4–7 times till convergence (reaction moments < 0.1 Nm). The nonlinear analyses and the optimization process are performed using ABAQUS 6.14 (Explicit: Quasi-static) and MATLAB (please see the Supplementary Materials section (Fig. 6) for more details).

3. Results

3.1. Optimal in situ strain distributions (optimization output)

The non-uniform optimal *in situ* strain distributions of the ligaments were predicted using the genetic algorithm. These non-uniform *in situ* strains were distributed over six areas on the ACL, two areas on the PCL, eighteen areas on the MCL, three areas on the LCL, two areas on the LPFL, and two areas on the MPFL (Fig. 2). We calculated the average *in situ* strains of 1.2%, 2%, 0.44%, 0.26%, 2.1%, 1.5%, 0.34%, and 0.76% for the anteromedial bundle (am-ACL), posterolateral bundle (pl-ACL), anterolateral bundle (al-PCL), posteromedial bundle (pm-PCL), MCL, LCL, LPFL, and MPFL, respectively. The minimum and maximum *in situ* strain values of approximately 0.04% and approximately 5.7% were predicted in the distal-posterior and middle-proximal areas of the MCL, respectively. These strains were calculated at the initial condition, where the joint was oriented at full extension position corresponding to the minimum activation of the muscle forces surrounding the knee joint. At equilibrium (when the joint is almost free from any external load), the *in situ* strains generated 36 N, 18 N, and 19 N as ACL, MCL, and LCL forces, respectively (Fig. 3a). The PCL force was less than 1 N, and lower forces, such as 2.4 N in the LPFL and 1.8 N in the MPFL, were also predicted in the patellofemoral ligaments. With the contact parameters shown in Fig. 3b, a peak contact force of 46 N occurred on the medial plateau and led to the maximum contact stress value in the uncovered area (cartilage–cartilage) of 0.3 MPa. However, a smaller contact force was predicted on the lateral plateau (approximately 34 N) and was mostly supported by the covered area (menisci-cartilage). On the lateral plateau, the contact area was slightly greater by 6% compared with the medial one.

3.2. Axial compression

Considering the optimal configuration of the *in situ* strains (Fig. 2) at full knee extension and under 2000 N of axial compression, the relative displacements of the joint decreased by approximately 1, 0.3, and 0.2 mm in the anterior, lateral, and proximal directions, respectively (Fig. 4a). Accordingly, a peak ligament force of 105 N was supported by the ACL and decreased to 96 N with the optimal configuration (with *in situ* strains). Under the same loading condition, the force in the collateral ligaments (MCL and LCL) was augmented by approximately 11%. Less than 5 N was computed for the rest of the ligaments (Fig. 4a). However, the inclusion of the *in situ* strains had a negligible effect on the predicted contact force/area, with a difference of less than 2%. This led to approximately the same cartilage stress/strain distributions within the contact region (Fig. 4b and d).

3.3. Knee flexion

During passive knee flexion, the PCL force increased and reached its peak at 16 N and 90° (Fig. 5a). However, the consideration of the ligament *in situ* strains substantially affected the PCL force only between the flexion range of 20–60°. The LCL exhibited the same trend as the PCL, but reached a maximum value of 42 N by 80° and increased to 53 N with optimal configuration (Fig. 5e). The ACL and MCL forces (Fig. 5b and d) were slightly affected by considering the *in situ* strains. However, a clear difference was observed between the calculated forces of the different bundles of the ACL structure when considering the case with and without *in situ* ligament strains (Fig. 5c and f). The total contact force increased with the ligament *in situ* strains, particularly in the knee flexion range of 20–60°. Eventually, the effect became more accentuated

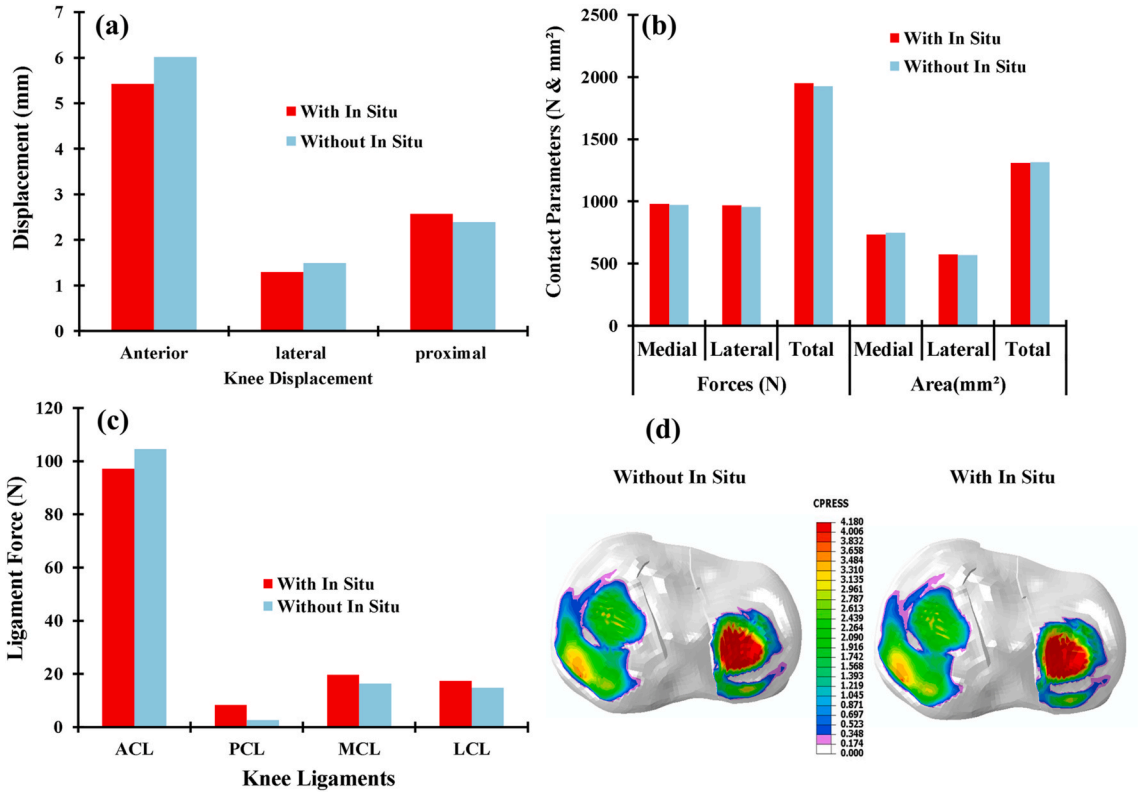

Fig. 4. The predicted tibiofemoral displacements (a), contact force and area (b), ligament forces (c), and contact stress (d) for the knee joint under 2000 N axial compression with and without ligaments *in situ* strain.

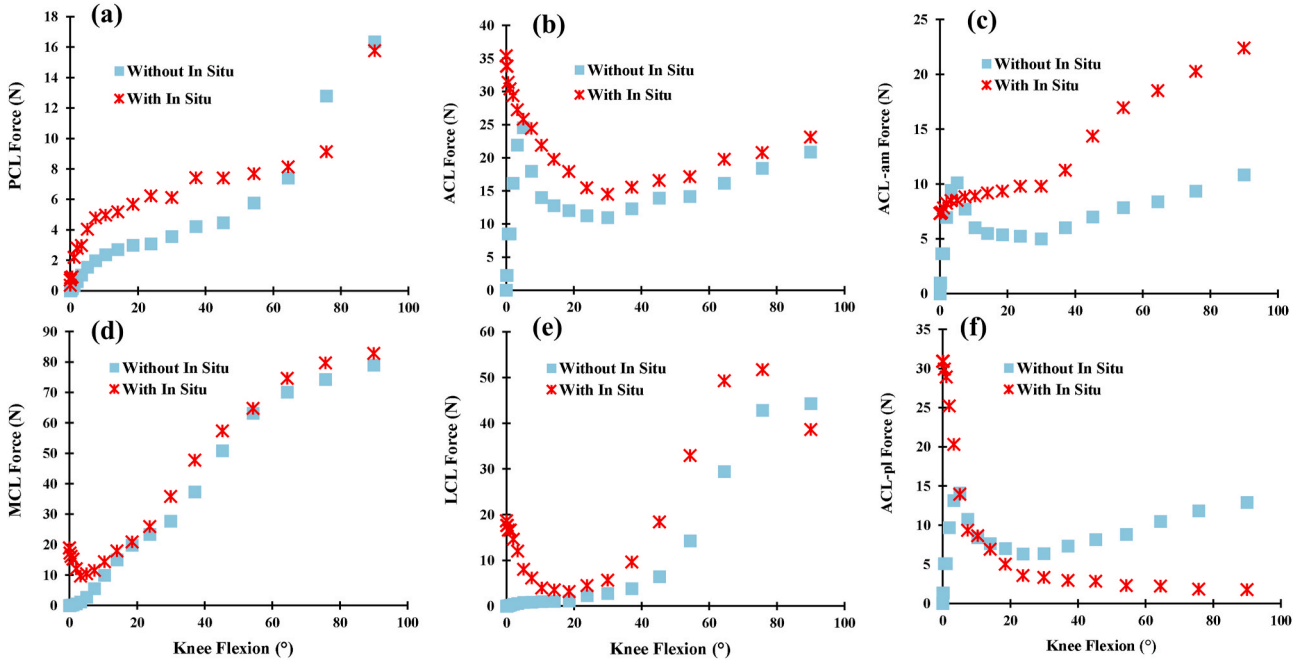

Fig. 5. The predicted ligaments forces (PCL (a), ACL (b), ACL-am(anteromedial bundle) (c), MCL (d), LCL (e), ACL-pl (posterolateral bundle) (f)) of the knee joint during knee flexion with and without ligaments *in situ* strain.

in the lateral plateau compared with that in the medial plateau (Fig. 6).

3.4. Adduction and internal rotations

The application of the *in situ* strains resulted in a much stiffer moment-rotation response under secondary coupled rotation (adduction and internal rotations; Fig. 7). As an extreme example, the adduction and internal moment increased by 50% and 80% at 6° and 10° of pure adduction and internal rotations, respectively.

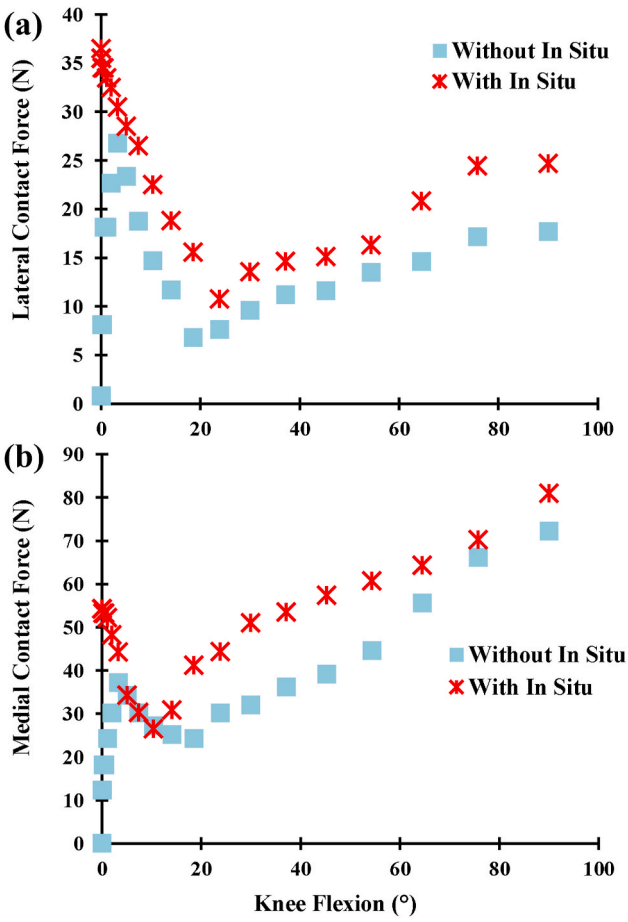

Fig. 6. The predicted lateral (a) and medial (b) tibiofemoral contact forces during knee flexion with and without ligaments *in situ* strain.

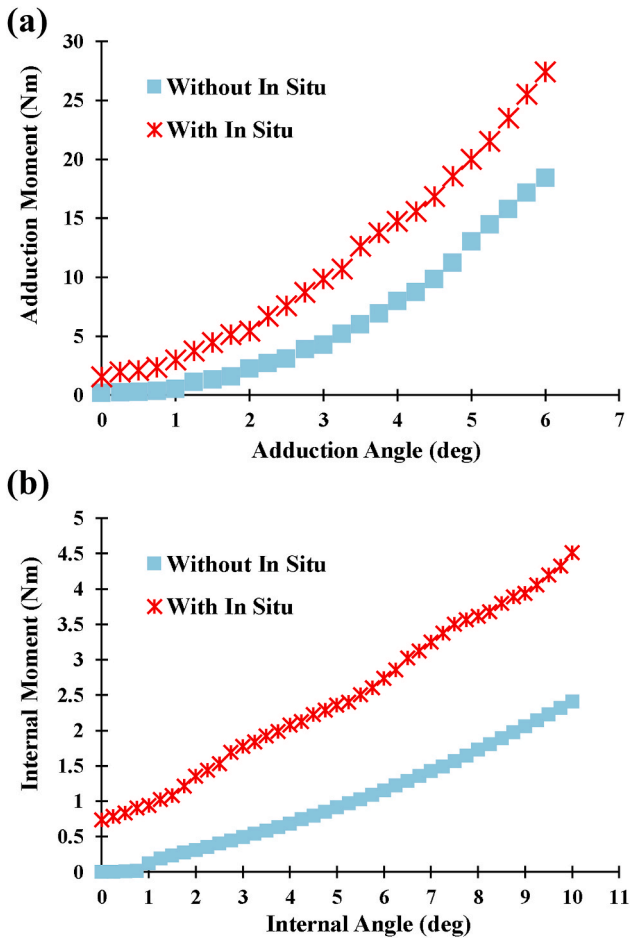

Fig. 7. The predicted moment-rotation curves in adduction (a) and internal (b) orientation at full extension with and without ligaments *in situ* strain.

3.5. Stance phase of gait

The exclusion of the *in situ* strains at the 0% and 50% instances slightly decreased the biomechanical response of the knee joint (Figs. 8 and 9). Moreover, the existence of ligament *in situ* strains in the joint exerted a negligible effect on the predicted muscle forces. However, the maximum contact pressure increased by approximately 9% and 8% on the lateral and medial plateaus at the 0% and 50% instances, respectively. In the other simulated instances (25, 75, and 100%), the consideration of the *in situ* strains substantially increased the predicted forces of the muscle surrounding the knee joint, such as the biceps femoris and semimembranosus, and these forces were augmented by approximately 30% and 35%, respectively, at the 25% instance of the stance phase (Fig. 8). Both the calculated total contact force and contact area at these instances increased by 20% on average (Fig. 9). On the side of the ligaments, only the ACL force increased significantly by an average of 28% (Fig. 9), with slight modifications for the rest of the ligaments.

4. Discussion

This study implemented a new computational framework to predict the effect of *in situ* strains in knee joint ligaments using the deformed reference configuration theory and a full knee FE model accounting for anatomically active and passive components. To investigate the effect of the estimated *in situ* strains, the net model of the knee joint was simulated with and without the *in situ* strains under 2000 N of axial compression, passive adduction rotation, passive internal rotation, passive flexion from full extension to 90°, and five instances (0, 25, 50, 75, and 100%) of the gait's stance phase. To the best of our knowledge, previous studies have not conducted a detailed investigation to gain insight into the full knee joint passive-active response in gait and isolated tasks. The results predicted by this study confirm the earlier observation of the non-uniform distribution of the *in situ* strains within the ligament structure. The inclusion of the ligament *in situ* strains significantly changed the net biomechanical response of the joint, particularly under pure adduction and internal rotations, for three instances (25, 75, and 100%) of the gait's stance phase.

The *in situ* strains reported in this study are supported by the data of previous experimental, computational, and clinical studies [3,42,43,53–57]. Gardiner and Weiss [3] have reported a similar trend in the strain distributions on the MCL at full knee extension in the absence of any external loading. The ligament *in situ* strain reached a maximum of 5.8% at the anterior proximal area close to the femoral insertion. The corresponding prediction was 5.7% and located in approximately the same region. However, the magnitudes of previously reported strains for the other areas comprising the MCL are higher than those predicted in this study. As an extreme case, we predicted a strain of approximately 0.04% for the distal posterior region, whereas previous studies have reported a strain of 2.5%. However, the remaining distributions are similar. For the ACL, the maximum strain of 3.1% was recorded in the inferior posterior area close to the tibial insertion. The posterolateral bundle of the ACL was more pre-strained compared with the anteromedial bundle. These results are consistent with the strains measured on the ACL bundles [43]. However, a contradictory observation has been reported by Grood and Hefzy [53] and Beynnon and Fleming [58] on the bundle strain distributions at a free strain state. The difference

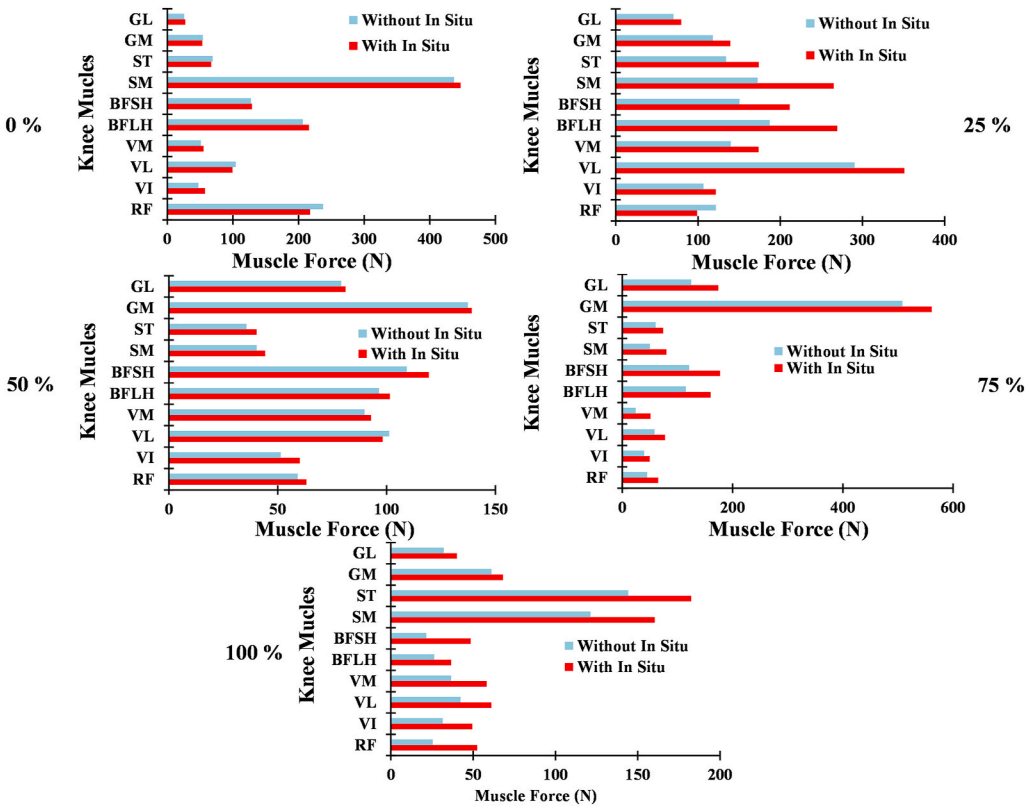

Fig. 8. The predicted muscle forces surrounding the knee joint during the five instances (0%, 25%, 50%, 75%, and 100%) of the stance phase of gait with and without ligaments *in situ* strain, (GL; gastrocnemius lateral, GM; gastrocnemius medial, ST; semitendinosus, SM; semimembranosus, BFSH; bicep femoris short head, BFLH; biceps femoris long head, VM; vastus medialis, VL; Vastus lateralis, VI; vastus intermedius, RF; rectus femoris).

may be attributed to the accuracy of used gage, the materials used to stick the gage on the ligament, and the little gap on the map of the *in situ* strains distribution since, in the present study, the MCL was more refined compared with published studies. The PCL remained almost slack at full extension, which is in good agreement with the results reported by most previous studies [54,55,59]. The LCL *in situ* strains reached a peak of 3.6% in the posterior region and gradually decreased in other areas. This result is corroborated by Wismans et al., [57]. Generally, the average in *situ* strain predicted in this study ranged from approximately 0.04%–5.7%, which falls within the bounds of previously reported measurements and material properties considered in various computational models [3,46,60].

The ligament *in situ* strain distributions calculated in this study led to the auto-balance of the knee joint without any externally applied load. This auto-balance is characterized by slake PCL and approximately slake patellofemoral ligaments. A peak ligament force of approximately 36 N was recorded on the ACL, followed by the LCL with a force equal to approximately 18 N, which appears to agree with the results obtained by previous experimental and modeling studies [42,43]. Moglo and Shirazi [61] have also reported ligament forces and contact parameters at full extension in the absence of any external loading. Their predictions were higher than the presented predictions. For instance, a greater ACL force (approximately 47 N) and a different contact force distribution associated with a higher lateral collateral ligament force were calculated. The direct comparison of their results with the results obtained by this study is complicated because the non-uniformity of the *in situ* strain was not established in their ligaments. Quantifying this onset loading map may help in overcoming the initial condition to resolve the force system characterizing the knee joint in rigid body modeling [62]. Additionally, this initial tautness may represent a baseline for targeting an optimal joint state by applying appropriate graft pre-tension during joint surgical reconstructive surgery, such as ACL replacement [63].

During the passive flexion of the tibiofemoral joint, the *ACL* force reached the maximum values of 36 N and 24 N at approximately full extension with and without ligament *in situ* strains, respectively (Fig. 5). This force diminished during flexion and reached approximately the same minimum (20 N) in both cases (with and without *in situ* strain). This result appears to be consistent with previously observed small forces in the ACL throughout the flexion range [64–66]. This ACL force variation during flexion was almost equally supported between the ACL bundles in the absence of *in situ* strains. However, by considering the optimal map of the *in situ* strain distribution, the ACL force was mostly supported by the ACL-pl bundle at full extension and gradually shifted to ACL-am with knee flexion. This trend is in agreement with previously reported measurements [7]. The results of this study were also confirmed by the reported measured increase in the ACL-am strain with knee joint flexion higher than 40° [42,43]. Moreover, the force in the PCL initiated with the joint flexion and reached 16 N at 90°. This result is consistent with the results obtained by previous studies that have reported the augmentation of PCL force/strain during knee flexion [54, 66–69]. The *in situ* strain in the PCL increased the stiffness of this ligament in the flexion range between full extension and 60°. In the collateral ligaments, LCL and MCL, the forces increased with the joint flexion, which provides a clear indication of their significant role at larger flexion angles. These findings corroborate those of Hull et al. [46], who reported a substantial strain increase in the MCL during knee flexion. However, the result obtained by this study is different to the previous observation of collateral ligament isometry reported by Victor et al. [70]. This difference is attributed to the slight deviation in the adopted boundary conditions (experimental set-up) and/or to certain weaknesses, which are mainly related to the technique used to measure the ligament length. The ligament *in situ* strain slightly affected the MCL force during flexion. However, higher resistance was observed in the LCL, particularly after 40° of flexion. Notably, most of the effects on the

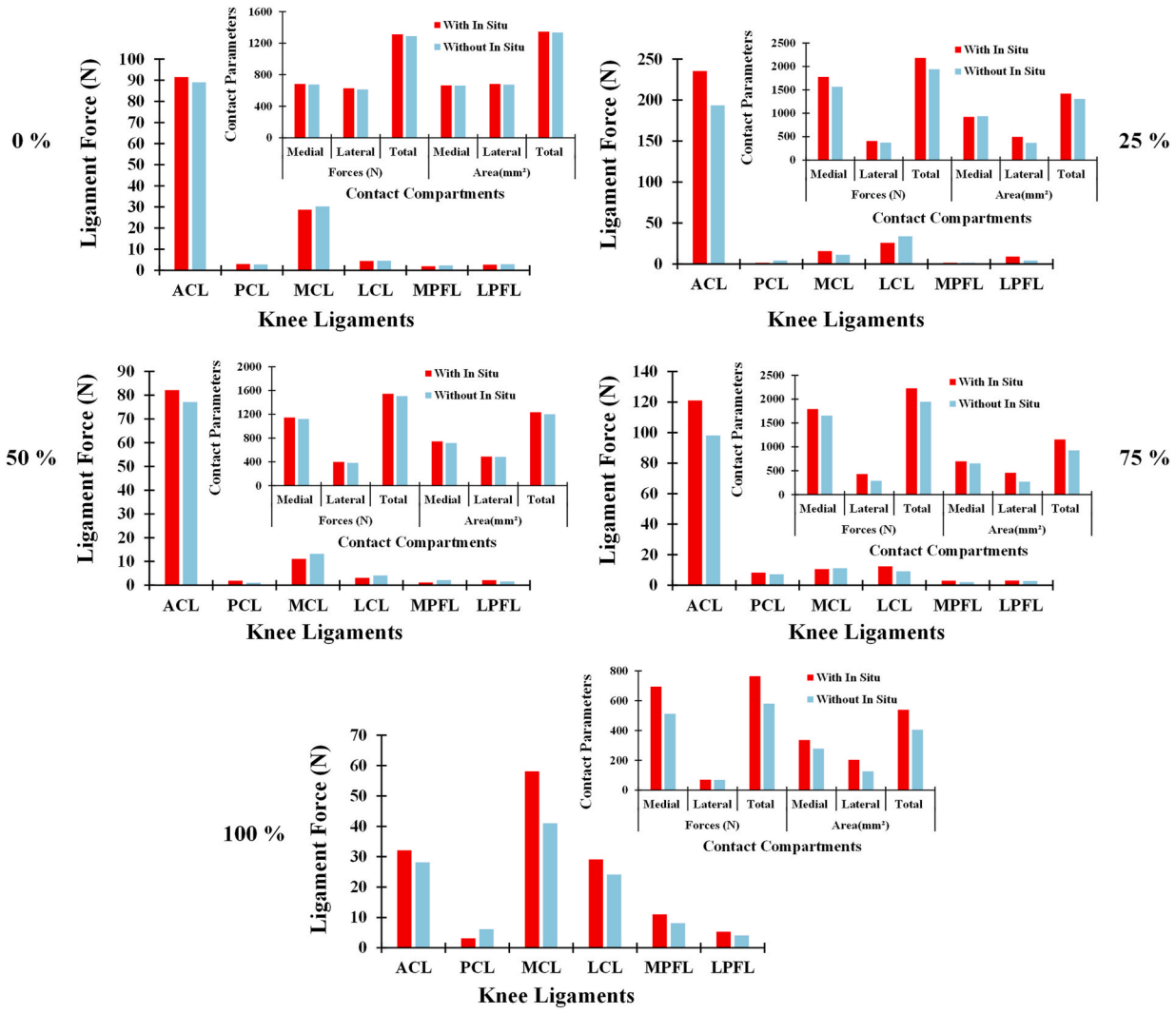

Fig. 9. The predicted ligaments forces, contact forces and areas for the knee joint during the five instances (0%, 25%, 50%, 75%, and 100%) of the stance phase of gait with and without ligaments *in situ* strain.

ligament forces when considering the *in situ* strains occurred in the range of 20°–60° of knee flexion. This justifies the greater contact force/stress calculated in the same flexion range when the *in situ* strains were considered (Fig. 6). One explanation for the more considerable change in the mechanics of the knee joint within the flexion range of 20°–60° is the screw-home mechanism. This is adequately characterized by the obvious augmentation of the coupled rotations (adduction and internal rotations) in the range of 10°–60° of flexion, which are considered as essential factors affecting the knee joint stiffness [71].

In this study, the slight increase in the mechanical response of the passive tissues was well documented during the knee joint simulation under the tibial axial loading of 2000 N in the presence of ligament *in situ* strains. This slight joint hardening can be explained by the associated changes in the joint kinematics (decrease in anterior/lateral/proximal translations). However, a slight decrease was calculated in the ACL force in the presence of *in situ* strains. This is attributed to the associated increase in the collateral ligament forces (MCL and LCL), which are considered as secondary restraints of anterior tibial translation. Our predicted results (with or without *in situ* strain) fall within the measured and calculated range of biomechanical variables during the axial knee compression in previous studies [33,71–73]. In contrast to the axial compression, the passive adduction and internal laxities of the knee joint substantially decreased by considering the *in situ* ligament strains. In other words, a significant augmentation of the tibiofemoral passive moment resistance was calculated on both sides (adduction and internal) at the same angulations (Fig. 7). This stiffer reaction of the joint is supported by the data of previous experimental, computational, and clinical studies [71,74–79] (please see supplementary materials section: model validation, Figs. 7–12).

The simulated instances of the gait's stance phase exhibited the insensitivity of the predicted muscle forces, ligament forces, average contact pressure, and area to the ligaments' *in situ* strains at the 0% and 50% instances. However, the presence of the ligament *in situ* strains in the other instances (25, 75, and 100%) of the stance phase significantly increased the muscle forces and led to the obvious augmentation of the predicted ligament forces, compartmental and total contact forces, areas, and contact stresses/strains. Therefore, the accentuated role (stiffer joint) caused by the inclusion of the *in situ* strain may have originated from the unstable loading conditions driving the 25, 75, and 100% cases of the gait's stance phase (higher applied flexion and coupled rotations) and the cases of adduction and internal rotations. The more critical role of the *in situ* strain in the joint biomechanics under less stable boundary conditions has been extensively documented (Winkelstein, 2012). This observation is in good agreement with the results of a previous study that conducted comprehensive investigations into the biomechanics of the knee joint under passive conditions, which promote the underestimation of joint loading in the absence of any ligament *in situ* strain [50]. Unsurprisingly, the ligament *in situ* strains only had a

minor effect on the joint mechanics during the relatively stable loading conditions, such as the 0% and 50% instances of the stance phase, axial compression, and passive flexion. This result is also consistent with the results obtained by previous studies, which did not provide evidence for the overestimation or underestimation of the joint stiffness when the ligament *in situ* strains were omitted [59,80]. Thus, our observations provide an insight into the importance of determining the best set of *in situ* strains and their necessity. For example, the consideration of this parameter appears ineffective or minimal when attempting to calculate the aggregate mechanics of the joint with very low kinematics on the frontal and transversal plan of the joint, but is highly relevant in other loading situations. Furthermore, the sub-loading state of the ligament, such as the case of the ACL bundle loading distribution during knee flexion, was significantly altered by the absence of *in situ* ligament strains.

Notably, the results and conclusions of this study are circumscribed by a few limitations. One of these limitations is the consideration of the nearly incompressible hyperelastic behavior of the connective tissues instead of biphasic–viscoelastic behavior. However, it has been extensively documented that the transient response of the soft tissue can be accurately captured either by biphasic–viscoelastic analysis or equivalently by nearly incompressible hyperelastic analysis [34]. Another limitation is the consideration of a generalized knee model obtained from a single joint while ignoring patient-specific knee models. The lack of experimental data for the ligament *in situ* strain distributions and their effects on the joint's biomechanical variables of interest, such as the ligament forces and contact parameters, are also considered as limitations. Furthermore, the sensitivity of the calculated results to the difference in the boundary conditions and material properties was not considered during this investigation. Nevertheless, our predicted results fall within the physiological range reported by previous studies [3,4,7,8,42,43,45,46,50].

In summary, the ligament *in situ* strains predicted using the proposed iterative framework were found to be in good agreement with those reported in the literature, which range from 1% to 10%. Generally, and as expected, the application of the ligament *in situ* strain resulted in the stiffer response of the knee joint, and therefore improved the joint stability. Our data also demonstrate that the inclusion of the ligament *in situ* strain in the knee model is often necessary to obtain reasonable estimates for the subsequent loading conditions of interest. The proposed construct may play a significant role in elucidating the functional biomechanics of human knee ligaments, which is critical for assessing and improving the prevention evaluation and treatment procedures for related disorders and injuries. Finally, the methodologies developed in this study can be easily adapted to investigate the initial configuration of other soft tissues and joints.

Author contributions

All authors have read and approved this submission; M.A. carried out analyses, all (M.A, T.F and Y.D) participated in the definition, design, and development of the work, and finally manuscript was written by all authors (M.A, T.F and Y.D).

Ethical approval

Not required.

Declaration of competing interest

There is no conflict of interest to declare.

Acknowledgment

This work is supported by a grant (#U01 EB015410-01A1) from the National Institute of Health NIH.

Appendix A. Supplementary data

Supplementary data to this article can be found online at https://doi.org/10.1016/j.compbiomed.2020.104012.

References

[1] A.A. Amis, P. Firer, J. Mountney, W. Senavongse, N.P. Thomas, Anatomy and biomechanics of the medial patellofemoral ligament, Knee 10 (2003) 215–220.
[2] H. Fujie, G.A. Livesay, S.L.Y. Woo, S. Kashiwaguchi, G. Blomstrom, The use of a universal force-moment sensor to determine in-situ forces in ligaments - a new methodology, Journal of Biomechanical Engineering-Transactions of the Asme 117 (1995) 1–7.
[3] J.C. Gardiner, J.A. Weiss, Subject-specific finite element analysis of the human medial collateral ligament during valgus knee loading, J. Orthop. Res. 21 (2003) 1098–1106.
[4] A. Kanamori, M. Sakane, J. Zeminski, T.W. Rudy, S.L. Woo, In-situ force in the medial and lateral structures of intact and ACL-deficient knees, J. Orthop. Sci. 5 (2000) 567–571.
[5] A. Kanamori, T. Vogrin, M. Yagi, M. Janaushek, S. Woo, C. Harner, Effects of PCL-deficiency on the soft tissues of the knee and joint contact forces, Trans Orthop Res Soc 25 (2000) 485.
[6] K.L. Markolf, M.J. Willems, S.R. Jackson, G.A.M. Finerman, In situ calibration of miniature sensors implanted into the anterior cruciate ligament part I: strain measurements, J. Orthop. Res. 16 (1998) 455–463.
[7] S.L.Y. Woo, R.J. Fox, M. Sakane, G.A. Livesay, T.W. Rudy, F.H. Fu, Biomechanics of the ACL: measurements of in situ force in the ACL and knee kinematics, Knee 5 (1998) 267–288.
[8] E. Pena, M.A. Martinez, B. Calvo, M. Doblare, On the numerical treatment of initial strains in biological soft tissues, Int. J. Numer. Methods Eng. 68 (2006) 836–860.
[9] F. Galbusera, M. Freutel, L. Dürselen, M. D'Aiuto, D. Croce, T. Villa, V. Sansone, B. Innocenti, Material models and properties in the finite element analysis of knee ligaments: a literature review, Frontiers in bioengineering and biotechnology 2 (2014) 54.
[10] S.L. Woo, J.A. Weiss, M.A. Gomez, D.A. Hawkins, Measurement of changes in ligament tension with knee motion and skeletal maturation, J. Biomech. Eng. 112 (1990) 46–51.
[11] B.J. Ellis, T.J. Lujan, M.S. Dalton, J.A. Weiss, Medial collateral ligament insertion site and contact forces in the ACL-deficient knee, J. Orthop. Res. 24 (2006) 800–810.
[12] T.J. Lujan, M.S. Dalton, B.M. Thompson, B.J. Ellis, J.A. Weiss, Effect of ACL deficiency on MCL strains and joint kinematics, J. Biomech. Eng. 129 (2007) 386–392.
[13] J. Vossoughi, Z. Hedjazi, F. Borris, Intimal residual stress and strain in large arteries, ASME-PUBLICATIONS-BED 24 (1993), 434-434.
[14] V. Alastrue, E. Pena, M.A. Martinez, M. Doblare, Assessing the use of the "Opening angle method" to enforce residual stresses in patient-specific arteries, Ann. Biomed. Eng. 35 (2007) 1821–1837.
[15] Y.Y. Dhaher, T.H. Kwon, M. Barry, The effect of connective tissue material uncertainties on knee joint mechanics under isolated loading conditions, J. Biomech. 43 (2010) 3118–3125.
[16] H. Weisbecker, D.M. Pierce, G.A. Holzapfel, A generalized prestressing algorithm for finite element simulations of preloaded geometries with application to the aorta, Int J Numer Method Biomed Eng 30 (2014) 857–872.
[17] R. Grytz, J.C. Downs, A forward incremental prestressing method with application to inverse parameter estimations and eye-specific simulations of posterior scleral shells, Comput. Methods Biomech. Biomed. Eng. 16 (2013) 768–780.
[18] T.L. Donahue, M.L. Hull, M.M. Rashid, C.R. Jacobs, A finite element model of the human knee joint for the study of tibio-femoral contact, J. Biomech. Eng. 124 (2002) 273–280.
[19] X. Bi, X. Yang, M.P. Bostrom, N.P. Camacho, Fourier transform infrared imaging spectroscopy investigations in the pathogenesis and repair of cartilage, Biochim. Biophys. Acta 1758 (2006) 934–941.
[20] H.U. Staubli, L. Schatzmann, P. Brunner, L. Rincon, L.P. Nolte, Mechanical tensile properties of the quadriceps tendon and patellar ligament in young adults, Am. J. Sports Med. 27 (1999) 27–34.
[21] T.L.H. Donahue, M.L. Hull, M.M. Rashid, C.R. Jacobs, How the stiffness of meniscal attachments and meniscal material properties affect tibio-femoral contact pressure computed using a validated finite element model of the human knee joint, J. Biomech. 36 (2003) 19–34.
[22] T.L.H. Donahue, M.L. Hull, M.M. Rashid, C.R. Jacobs, The sensitivity of tibiofemoral contact pressure to the size and shape of the lateral and medial menisci, J. Orthop. Res. 22 (2004) 807–814.
[23] D. Skaggs, W. Warden, V. Mow, Radial tie fibers influence the tensile properties of the bovine medial meniscus, J. Orthop. Res. 12 (1994) 176–185.
[24] M. Tissakht, A. Ahmed, Tensile stress-strain characteristics of the human meniscal material, J. Biomech. 28 (1995) 411–422.
[25] J. Yao, P.D. Funkenbusch, J. Snibbe, M. Maloney, A.L. Lerner, Sensitivities of medial meniscal motion and deformation to material properties of articular cartilage, meniscus and meniscal attachments using design of experiments methods, J. Biomech. Eng. 128 (2006) 399–408.
[26] J.M. Penrose, G.M. Holt, M. Beaugonin, D.R. Hose, Development of an accurate three-dimensional finite element knee model, Comput. Methods Biomech. Biomed. Eng. 5 (2002) 291–300.

[27] M.M. Hoffer, A primer of orthopaedic biomechanics, J. Am. Med. Assoc. 249 (1983), 2397-2397.
[28] M.J. Buehler, R. Ballarini, Materiomics: Multiscale Mechanics of Biological Materials and Structures, Springer, 2013.
[29] H. Tang, M.J. Buehler, B. Moran, A constitutive model of soft tissue: from nanoscale collagen to tissue continuum, Ann. Biomed. Eng. 37 (2009) 1117–1130.
[30] M. Adouni, Y.Y. Dhaher, A multi-scale elasto-plastic model of articular cartilage, J. Biomech. 49 (2016) 2891–2898.
[31] M. Adouni, T.R. Faisal, M. Gaith, Y.Y. Dhaher, A multiscale synthesis: characterizing acute cartilage failure under an aggregate tibiofemoral joint loading, Biomech. Model. Mechanobiol. (2019).
[32] T.R. Faisal, M. Adouni, Y.Y. Dhaher, The effect of fibrillar degradation on the mechanics of articular cartilage: a computational model, Biomech. Model. Mechanobiol. (2019) 1–19.
[33] R. Shirazi, A. Shirazi-Adl, M. Hurtig, Role of cartilage collagen fibrils networks in knee joint biomechanics under compression, J. Biomech. 41 (2008) 3340–3348.
[34] G.A. Ateshian, B.J. Ellis, J.A. Weiss, Equivalence between short-time biphasic and incompressible elastic material responses, Journal of Biomechanical Engineering-Transactions of the Asme 129 (2007) 405–412.
[35] R.M. Schinagl, D. Gurskis, A.C. Chen, R.L. Sah, Depth-dependent confined compression modulus of full-thickness bovine articular cartilage, J. Orthop. Res. 15 (1997) 499–506.
[36] G. Limbert, J. Middleton, A transversely isotropic viscohyperelastic material - application to the modeling of biological soft connective tissues, Int. J. Solid Struct. 41 (2004) 4237–4260.
[37] M.J. Schroeder, A Computational Framework to Evaluate the Efficacy of Anterior Cruciate Ligament Reconstruction Procedures. Biomedical Engineering, Northwestern university, Evanston, illinois, 2010.
[38] M.J. Schroeder, A Multi-Domain Synthesis of Neuromechanical Adaptations Post Anterior Cruciate Ligament Reconstructive Surgery. *Biomedical Engineering*, Northwestern university, Evanston, illinois, 2014.
[39] M.J. Schroeder, C. Krishnan, Y.Y. Dhaher, The influence of task complexity on knee joint kinetics following ACL reconstruction, Clin. Biomech. 30 (2015) 852–859.
[40] J.A. Weiss, B.N. Maker, D.A. Schauer, Treatment of initial stress in hyperelastic finite element models of soft tissues, in: Proceedings of the 1995 Bioengineering Conference, ASME, Winkelstein, B.A., 2012. Orthopaedic Biomechanics, CRC Press, 1995.
[41] S.A. Maas, A. Erdemir, J.P. Halloran, J.A. Weiss, A general framework for application of prestrain to computational models of biological materials, J Mech Behav Biomed Mater 61 (2016) 499–510.
[42] J.M. Bach, M.L. Hull, Strain inhomogeneity in the anterior cruciate ligament under application of external and muscular loads, J. Biomech. Eng. 120 (1998) 497–503.
[43] J.M. Bach, M.L. Hull, H.A. Patterson, Direct measurement of strain in the posterolateral bundle of the anterior cruciate ligament, J. Biomech. 30 (1997) 281–283.
[44] J. Chahla, K.N. Kunze, J.P. Fulkerson, A. Yanke, Lateral patellofemoral ligament reconstruction: anatomy, biomechanics, indications and surgical techniques, Operat. Tech. Sports Med. 27 (2019) 150689.
[45] J.C. Gardiner, J.A. Weiss, T.D. Rosenberg, Strain in the human medial collateral ligament during valgus loading of the knee, Clin. Orthop. Relat. Res. 391 (2001) 266–274.
[46] M.L. Hull, G.S. Berns, H. Varma, H.A. Patterson, Strain in the medial collateral ligament of the human knee under single and combined loads, J. Biomech. 29 (1996) 199–206.
[47] E. Hunziker, Structural Molecules in Articular Cartilage, Tendons, and Ligaments. The Knee and the Cruciate Ligaments, Springer, 1992, pp. 62–77.
[48] T.C. Telger, R.P. Jakob, H.-U. Stäubli, The Knee and the Cruciate Ligaments: Anatomy Biomechanics Clinical Aspects Reconstruction Complications Rehabilitation, Springer Science & Business Media, 2012.
[49] C.-h. Wang, L.-f. Ma, J.-w. Zhou, G. Ji, H.-y. Wang, F. Wang, J. Wang, Double-bundle anatomical versus single-bundle isometric medial patellofemoral ligament reconstruction for patellar dislocation, Int. Orthop. 37 (2013) 617–624.
[50] J.A. Weiss, J.C. Gardiner, Computational modeling of ligament mechanics, Crit. Rev. Biomed. Eng. 29 (2001) 303–371.
[51] M. Adouni, A. Shirazi-Adl, Evaluation of knee joint muscle forces and tissue stresses-strains during gait in severe OA versus normal subjects, J. Orthop. Res. 32 (2014) 69–78.
[52] M. Adouni, A. Shirazi-Adl, R. Shirazi, Computational biodynamics of human knee joint in gait: from muscle forces to cartilage stresses, J. Biomech. 45 (2012) 2149–2156.
[53] Grood, M. Hefzy, An analytical technique for modeling knee joint stiffness—Part I: ligamentous forces, J. Biomech. Eng. 104 (1982) 330.
[54] J. Hoher, T.M. Vogrin, S.L. Woo, G.J. Carlin, A. Aroen, C.D. Harner, In situ forces in the human posterior cruciate ligament in response to muscle loads: a cadaveric study, J. Orthop. Res. 17 (1999) 763–768.
[55] G. Li, T.J. Gill, L.E. DeFrate, S. Zayontz, V. Glatt, B. Zarins, Biomechanical consequences of PCL deficiency in the knee under simulated muscle loads - an in vitro experimental study, J. Orthop. Res. 20 (2002) 887–892.
[56] W. Mesfar, A. Shirazi-Adl, Knee joint mechanics under quadriceps–hamstrings muscle forces are influenced by tibial restraint, Clin. Biomech. 21 (2006) 841–848.
[57] J. Wismans, F. Veldpaus, J. Janssen, A. Huson, P. Struben, A three-dimensional mathematical model of the knee-joint, J. Biomech. 13 (1980) 677–685.
[58] B.D. Beynnon, B.C. Fleming, Anterior cruciate ligament strain in-vivo: a review of previous work, J. Biomech. 31 (1998) 519–525.
[59] W. Mesfar, A. Shirazi-Adl, Biomechanics of changes in ACL and PCL material properties or prestrains in flexion under muscle force-implications in ligament reconstruction, Comput. Methods Biomech. Biomed. Eng. 9 (2006) 201–209.
[60] M. Bendjaballah, A. Shirazi-Adl, D. Zukor, Biomechanics of the human knee joint in compression: reconstruction, mesh generation and finite element analysis, Knee 2 (1995) 69–79.
[61] K.E. Moglo, A. Shirazi-Adl, Cruciate coupling and screw-home mechanism in passive knee joint during extension–flexion, J. Biomech. 38 (2005) 1075–1083.
[62] S.L. Delp, F.C. Anderson, A.S. Arnold, P. Loan, A. Habib, C.T. John, E. Guendelman, D.G. Thelen, OpenSim: open-source software to create and analyze dynamic simulations of movement, IEEE Trans. Biomed. Eng. 54 (2007) 1940–1950.
[63] Y.Y. Dhaher, S. Salehghaffari, M. Adouni, Anterior laxity, graft-tunnel interaction and surgical design variations during anterior cruciate ligament reconstruction: a probabilistic simulation of the surgery, J. Biomech. 49 (2016) 3009–3016.
[64] K.L. Markolf, J.F. Gorek, J.M. Kabo, M.S. Shapiro, Direct measurement of resultant forces in the anterior cruciate ligament. An in vitro study performed with a new experimental technique, J Bone Joint Surg Am 72 (1990) 557–567.
[65] S. Takai, S.L. Woo, G.A. Livesay, D.J. Adams, F.H. Fu, Determination of the in situ loads on the human anterior cruciate ligament, J. Orthop. Res. 11 (1993) 686–695.
[66] D.C. Wascher, K.L. Markolf, M.S. Shapiro, G.A. Finerman, Direct in vitro measurement of forces in the cruciate ligaments. Part I: the effect of multiplane loading in the intact knee, J Bone Joint Surg Am 75 (1993) 377–386.
[67] B. Beynnon, J. Yu, D. Huston, B. Fleming, R. Johnson, L. Haugh, M.H. Pope, A sagittal plane model of the knee and cruciate ligaments with application of a sensitivity analysis, J. Biomech. Eng. 118 (1996) 227–239.
[68] C.D. Harner, M.A. Janaushek, C.B. Ma, A. Kanamori, T.M. Vogrin, S.L.Y. Woo, The effect of knee flexion angle and application of an anterior tibial load at the time of graft fixation on the biomechanics of a posterior cruciate ligament-reconstructed knee, Am. J. Sports Med. 28 (2000) 460–465.
[69] K.L. Markolf, G. O'Neill, S.R. Jackson, D.R. McAllister, Effects of applied quadriceps and hamstrings muscle loads on forces in the anterior and posterior cruciate ligaments, Am. J. Sports Med. 32 (2004) 1144–1149.
[70] J. Victor, P. Wong, E. Witvrouw, J.V. Sloten, J. Bellemans, How isometric are the medial patellofemoral, superficial medial collateral, and lateral collateral ligaments of the knee? Am. J. Sports Med. 37 (2009) 2028–2036.
[71] H. Marouane, A. Shirazi-Adl, M. Adouni, Knee joint passive stiffness and moment in sagittal and frontal planes markedly increase with compression, Comput. Methods Biomech. Biomed. Eng. 18 (2015) 339–350.
[72] H.I. Inaba, M.A. Arai, W.W. Watanabe, Influence of the varus-valgus instability on the contact of the femoro-tibial joint, Proc. Inst. Mech. Eng. H 204 (1990) 61–64.
[73] M.B. Pohl, C. Lloyd, R. Ferber, Can the reliability of three-dimensional running kinematics be improved using functional joint methodology? Gait Posture 32 (2010) 559–563.
[74] M.Z. Bendjaballah, A. Shirazi-Adl, D.J. Zukor, Finite element analysis of human knee joint in varus-valgus, Clin. Biomech. 12 (1997) 139–148.
[75] D.G. Lloyd, T.S. Buchanan, Strategies of muscular support of varus and valgus isometric loads at the human knee, J. Biomech. 34 (2001) 1257–1267.
[76] K. Markolf, K. Yamaguchi, J. Matthew, D. McAllister, Effects of tibiofemoral compression on ACL forces and knee kinematics under combined knee loads, J. Orthop. Res. 37 (2019) 631–639.
[77] K.L. Markolf, W.L. Bargar, S.C. Shoemaker, H.C. Amstutz, The role of joint load in knee stability, J Bone Joint Surg Am 63 (1981) 570–585.
[78] H. Marouane, A. Shirazi-Adl, Sensitivity of medial-lateral load sharing to changes in adduction moments or angles in an asymptomatic knee joint model during gait, Gait Posture (2019).
[79] E.G. Meyer, R.C. Haut, Anterior cruciate ligament injury induced by internal tibial torsion or tibiofemoral compression, J. Biomech. 41 (2008) 3377–3383.
[80] M.S. Hortin, A.E. Bowden, Quantitative comparison of ligament formulation and pre-strain in finite element analysis of the human lumbar spine, Comput. Methods Biomech. Biomed. Eng. 19 (2016) 1505–1518.